

SAFE-GIL: SAFETy Guided Imitation Learning

Yusuf Umut Ciftci

University of Southern California
yciftci@usc.edu

Zeyuan Feng

University of Southern California
zeyuanfe@usc.edu

Somil Bansal

University of Southern California
somilban@usc.edu

Abstract—Behavior cloning is a popular approach to imitation learning, in which a robot observes an expert supervisor and learns a control policy. However, behavior cloning suffers from the “compounding error” problem – the policy errors compound as it deviates from the expert demonstrations and might lead to catastrophic system failures, limiting its use in safety-critical applications. On-policy data aggregation methods are able to address this issue at the cost of rolling out and repeated training of the imitation policy, which can be tedious and computationally prohibitive. We propose SAFE-GIL, an off-policy behavior cloning method that guides the expert via adversarial disturbance during data collection. The algorithm abstracts the imitation error as an adversarial disturbance in the system dynamics, injects it during data collection to expose the expert to safety critical states, and collects corrective actions. Our method biases training to more closely replicate expert behavior in safety-critical states and allows more variance in less critical states. We compare our method with several behavior cloning techniques and DAgger on autonomous navigation and autonomous taxiing tasks and show higher task success and safety, especially in low data regimes where the likelihood of error is higher, at a slight drop in the performance.

I. INTRODUCTION

Imitation learning offers a powerful framework for teaching robots complex behaviors without needing detailed reward signals. A key technique in this domain is Behavior Cloning, where a robot learns direct mappings from states or observations to actions by emulating a supervisor [29, 34]. Behavior cloning has been used across a variety of robotic applications, ranging from manipulation [12, 20], navigation [7], to autonomous driving [3, 29, 11, 28]. However, typically behavior cloning is an off-policy method that can suffer from compounding errors when the robot executes the learned policy, leading the system to drift to new and potentially dangerous states over time [30]. This issue is particularly critical in safety-sensitive robotic applications, such as self-driving cars, where these errors could lead to catastrophic system failures.

The compounding error in behavior cloning is fundamentally due to covariate shift, where initial minor errors cause the agent to encounter states it hasn’t been trained on, leading to increasingly significant errors. Several methods have been proposed in the literature to overcome this challenge. These methods can broadly be classified into off-policy, on-policy, and safety filtering techniques. Off-policy approaches diversify training with noise-augmented supervisor demonstrations to expose the system to potential state deviations [22]. However, these methods often overlook the “criticality” of a state

during noise injection. Indeed, a minor deviation in a high-risk scenario can have disproportionately severe consequences compared to a safer context. For example, a small amount of error in the policy of a drone flying next to a wall can be much more catastrophic compared to the middle of a hallway.

On-policy methods, such as DAgger, address covariate shift by iteratively aggregating the states visited by the imitation policy, collecting expert policy on these states, and then refining the imitation policy. While shown to be effective, this approach has several limitations: (a) repeatedly updating the robot’s policy online can be tedious and computationally expensive; (b) these methods do not *preempt* safety violations.

Safety filtering offers an alternative method to prevent critical failures by employing the learned policy unless it poses a safety risk, at which point a backup policy intervenes. However, safety filtering methods have two key challenges: (a) reliance on an alternative policy might impede the overall performance as they are generally optimized only for safety; (b) safety filters often depend on privileged information about the environment or robot state that may not be accessible in real deployment scenarios, limiting their practical utility.

We propose SAFE-GIL (SAFETy Guided Imitation Learning) – a novel off-policy, behavior cloning approach that strategically exposes the expert to safety-critical scenarios and learn corrective actions. Our key insight is to abstract the policy error as an adversarial disturbance in the system dynamics that attempts to steer the system into safety-critical states. By injecting such disturbances into expert demonstrations, we intentionally navigate the system towards riskier situations. Our hypothesis is that collecting expert demonstrations at such states will enhance the learned policy’s ability to recover from such incidents and preserve system safety during test time. To compute the adversarial disturbance, we use Hamilton-Jacobi reachability analysis, a formal verification method to quantify the criticality of a robot state. SAFE-GIL combines the advantages of off-policy methods, while prioritizing the enhancement in system safety under the learned policy.

We demonstrate SAFE-GIL on two different robotic tasks: autonomous navigation in an indoor environment and autonomous aircraft taxiing. Our results highlight that, compared to alternative approaches, SAFE-GIL achieves a substantially higher success rate using the same amount of demonstration data. This advantage is particularly pronounced in low data regimes, where the model’s high prediction error traditionally increases the risk of failure.

II. RELATED WORK

Behavior cloning approaches in imitation learning are widely acknowledged to be susceptible to the compounding error problem [30]. Various methods have been proposed to mitigate this issue, which fall into the categories of on-policy, off-policy, and safety-filtering approaches. We discuss some of the relevant approaches here.

A. On-Policy Methods to Address Covariate Shift

On-policy methods iteratively aggregate expert actions on states visited by the imitation policy online to match the expert and imitator distributions. The success of on-policy imitation learning methods traces back to DAgger [31], which achieves a robust imitation of the expert policy using aforementioned iterative online data aggregation. However, similar to alternative online methods, querying the expert online and updating the robot policy can be tedious and computationally expensive. Multiple methods have been proposed to reduce the number of queries to the expert for on policy imitation learning. SafeDAgger [35] only requests supervision on states where a learned policy deems unsafe during imitation rollouts and EnsembleDAgger [23] is another variation which uses a bayesian quantification to classify unsafe state. ThriftyDAgger [13] further incorporates both novelty and risk in such state assessment. Except determining optimal timing for querying expert action, LazyDAgger [14] enables the expert to provide supervision for a small number of contiguous states instead of one off state to action pairs. Similarly, Specification-Guided DAgger (SGDA) [32] identify partitions of the state space where the imitator behaves most differently from the expert. Nevertheless, all these methods still tradeoff querying efficiency and distribution matching quality. Furthermore, these methods do not preempt safety violations, making them challenging to use in safety-critical applications.

B. Off-Policy Methods to Address Covariate Shift

Off-policy methods address covariate shift by “reshaping” the training data distribution to yield a robust imitation policy. DART [22] iteratively injects noise during expert rollouts, then uses the learned policy to estimate the noise parameter that mimics the error between the demonstrator and the current imitation policy the best. However, such a learning scheme does not distinguish the safety importance of different state-action pairs. One key insight motivating our work is that it is more important to closely follow the expert policy in certain critical states, i.e., states where small deviations can lead to failure or unsafe behavior [21]. In other states, the tolerance for errors is higher and consequently a relatively rough approximation of the expert policy still allows the learner to complete the task. [16] proposed a measure of state criticality based on the variance of estimated Q-values across the action space, i.e. the states where Q-value varies substantially given different control actions are identified as critical. Instead of evaluating the safety risk in an approximate manner, we leverage Hamilton-Jacobi reachability analysis [5]

to measure the safety criticality of a state and obtain the disturbance that leads to maximum increase in the safety risk.

C. Safety Filtering Methods

An alternative approach to ensuring safety of the learned policy is safety filtering, where the learned policy is minimally adjusted (i.e., “filtered”) to satisfy the safety constraint. If the input is safe, it is used directly; otherwise, it is projected to a set of safe control inputs. This approach guarantees safety while optimizing performance whenever the system safety is not at risk. A number of approaches have been proposed in literature to construct safety filters for robotic systems, such as Control Barrier and Control Lyapunov functions [1], Hamilton-Jacobi reachability [2, 9], and MPC [33]. We refer the interested readers to [15] and [33] for a detailed survey on filtering methods. However, safety filtering can compromise the overall performance of the system [9]. Furthermore, constructing safety filters often require privileged information about the environment or robot state that may not be accessible during the test time.

III. PROBLEM SETUP

Consider an autonomous robot with state $x \in X \subseteq \mathbb{R}^n$ and control $u \in \mathcal{U}$. We also assume access to an approximate dynamics model of the robot $\dot{x} = f(x, u)$ during training time.

A policy or agent is a function that maps robot states or observations to controls. Let $\pi^*(\cdot)$ denote an expert policy that achieves a desired level of performance on the task. The expert is replicated by an imitation policy $\pi_\theta(\cdot)$, where $\theta \in \Theta$ can be learned by minimizing the mean squared error between the expert control and the imitator control. Finally, let L be a set of states that represent a failure for the robot. For example, L might represent obstacles for a navigation robot or off-runway positions for an autonomous aircraft.

Our goal is to answer how to best collect expert demonstrations $D = \{(x^{(i)}, \pi^*(x^{(i)})), i = 1, \dots, N\}$ so that an imitation policy $\pi_\theta(\cdot)$ trained on this data completes the desired task while keeping the robot safe (i.e., outside L). The key challenge in achieving this objective is the compounding error problem [30] caused by learning from offline expert demonstrations. In this work, we will use Hamilton-Jacobi reachability analysis to guide the robot toward safety-critical states and collect data that will help enhance the system safety under imitation policy.

Running example. We now introduce a running example that we will use throughout the paper to ground the key ideas. We consider a ground wheeled robot navigating in a 2D space to reach a goal position without colliding with obstacles in the environment. A schematic of the robot and its environment are shown in Fig. 3. The navigation task is to be performed autonomously starting from various initial states using an expert demonstrator.

The robot state is given by $x := (p_x, p_y, \theta)$, where (p_x, p_y) denote the position of the robot and θ represents its heading.

The robot is assumed to be moving at a constant speed $v = 1 \text{ m/s}$. The robot control input is given by its angular velocity $u := \omega$, which is bounded by the physical constraints of the vehicle's steering capability, i.e., $\omega \in [-\bar{\omega}, \bar{\omega}]$. Here, $\bar{\omega}$ can be interpreted as the maximum rate at which the robot can turn. In our example, we use $\bar{\omega} = 1 \text{ rad/s}$. We model the robot as a unicycle whose dynamics is given as:

$$\begin{aligned}\dot{p}_x &= v \cos(\theta), \\ \dot{p}_y &= v \sin(\theta), \\ \dot{\theta} &= \omega\end{aligned}$$

The failure set L is given by the obstacles (highlighted in gray in Fig. 3) that the robot must avoid on its way to the goal. The expert here employs Model Predictive Control (MPC) to obtain the optimal control sequence that minimizes the following cost function penalizing the robot's distance to the goal location, obstacle penetration, and control energy.

$$J(\xi, u) = \sum_{i=0}^T J_i(x_i, u_i) \quad (1)$$

$$J_i(x_i, u_i) := d^{goal}(x_i) + c_{obs1} \exp(-c_{obs2} d^{obs}(x_i)) + c_{energy} u_i^2 \quad (2)$$

where ξ is the state trajectory, u is the corresponding control sequence, and T is the planning horizon. $d^{goal}(x_i)$ is the minimum collision-free distance to the goal position computed using the fast marching method, and $d^{obs}(x_i)$ is the signed distance to the obstacles. For MPC, we use 100 samples at each planning step with a horizon of 5 steps, and discretize the robot dynamics with a $\Delta T = 0.1 \text{ s}$.

The imitation agent is to take as input the current robot state (p_x, p_y, θ) and outputs the angular speed for the robot in order to reach the goal while avoiding obstacles.

IV. BACKGROUND

We now provide a brief overview of Hamilton-Jacobi reachability analysis which will be crucial in the safety assessment of a robot state and computing adversarial disturbance to guide it towards safety-critical states.

A. Hamilton-Jacobi (HJ) Reachability

Hamilton-Jacobi (HJ) reachability analysis is a formal verification method for characterizing the safety properties of dynamical systems. Its advantages include compatibility with general nonlinear system dynamics, formal treatment of bounded disturbances, and the ability to deal with state and input constraints

For reachability analysis, we will consider a more general form of dynamics: $\dot{x} = f(x, u, d)$, where $d \in [-\bar{d}, \bar{d}]$ represents the disturbance. Later on, in our work, we will use d to model potential policy errors. Given the dynamics f and a failure set L , in reachability analysis, one is interested in computing the backward reachable tube (BRT) of the system

– the set of all states from which the system will eventually enter the failure set regardless of the control policy $u(\cdot)$, given the system is subject to optimum disturbance policy $d(\cdot)$ [6]. Hamilton-Jacobi (HJ) reachability formulates the BRT computation as a robust optimal control problem, where the disturbance tries its best to steer the system towards L and the control tries to keep the system safe. This game can be solved using the dynamic programming principle, which we describe next.

First, a Lipschitz continuous target function $l(x)$ is defined whose sub-zero level set is the failure set L , i.e. $L = \{x : l(x) \leq 0\}$. Then we can formulate the cost function for the robust optimal control problem as the minimum value of target function achieved by the trajectory starting from the state x , for the time horizon $[t, T]$ under the control policy $u(\cdot)$ and disturbance policy $d(\cdot)$.

$$J(x, t, u(\cdot), d(\cdot)) = \min_{\tau \in [t, T]} l(\xi(\tau; x, t, u(\cdot), d(\cdot))). \quad (3)$$

Under non-anticipative strategies, where optimal $u(\cdot)$ drives the system away from the unsafe states and optimal $d(\cdot)$ drives the system towards them, the robust value function can be obtained by solving the following final value Hamilton-Jacobi-Isaacs Variational Inequality (HJI-VI).

$$\min \{D_t V(x, t) + H(x, t), l(x) - V(x, t)\} = 0, \quad (4)$$

$$V(x, T) = l(x), \quad (5)$$

where D_t and ∇ represent the time and spatial gradients of the value function and H is the Hamiltonian, which optimizes over the inner product between the spatial gradients of the value function and the system dynamics to compute the optimal control and disturbance:

$$H(x, t) = \max_u \min_d \langle \nabla V(x, t), f(x, u, d) \rangle. \quad (6)$$

For a detailed derivation and discussion of the HJI-VI in 4, we refer the interested readers to [25] and [5].

Intuitively, the value function corresponding to the above robust optimal control problem provides a measure of safety for each state:

$$V(x, t) = \inf_{d(\cdot)} \sup_{u(\cdot)} J(x, t, u(\cdot), d(\cdot)). \quad (7)$$

The value function typically converges after some time horizon, beyond which the system has enough time to maneuver to avoid the failure set despite the worst case disturbance. Consequently, we can use the converged value function, which is no longer a function of time t ,

$$V^*(x) = \lim_{t \rightarrow \infty} V(x, t). \quad (8)$$

Once the value function is obtained, the BRT is given as the sub-zero level set of the value function:

$$\mathcal{V} = \{x : V^*(x) \leq 0\}. \quad (9)$$

A lower value denotes a more safety critical state and a value below 0 denotes an unrecoverable state. Thus, the BRT

represents the set of all states from which the system cannot recover.

Moreover, we can synthesize the disturbance that optimally leads the agent to unsafe states, which is denoted as:

$$d^*(x) = \max_u \arg \min_d \langle \nabla V^*(x), f(x, u, d) \rangle \quad (10)$$

Intuitively, at each state x , $d^*(x)$ tries to steer the system in the direction of maximum descent in the value function. If $x \in \mathcal{V}$, d^* will eventually be successful in causing the failure, regardless of control applied. On the other hand, if the system state is outside \mathcal{V} , the controller can avert the failure. Nevertheless, d^* will still guide the system closest to the failure set to the extent possible.

B. HJ Reachability Computation

Several methods have been proposed to solve the HJI-VI in (4) and compute the value function (see [5] for a survey). One method is to numerically solve the HJB-VI over a discretized grid in the state space [24, 8], which is what we primarily use in this work to compute the value function, though other methods exist that are scalable to high-dimensional systems [4].

Running example. We compute the value function over the statespace: $[0, 10]m$ for p_x , $[0, 10]m$ for p_y , and $[-180^\circ, 180^\circ]$ for θ . We use a uniform grid $101 \times 101 \times 101$ along all dimensions and leverage the Level Set Toolbox [26, 27] to solve the HJB-VI numerically. The value function is computed separately for disturbance bounds $\bar{d} \in \{0.1, 0.2, 0.3, 0.4, 0.5, 0.6\} rad/s$. The value functions are propagated until convergence which happens after ≈ 17 seconds for this dynamical system model for all disturbance bounds. The computation time takes less than 25 seconds for each disturbance bound. A slice of the computed value function for the unicycle dynamics with $\bar{d} = 0.5$ can be seen in Fig. 1. The lower the value, the more unsafe the state is. Specifically, the areas with negative values contain the set of states from which the robot will eventually enter the obstacles (BRT of the system). On the other hand, positive value means safe states.

V. SAFE-GIL: SAFETY GUIDED IMITATION LEARNING

We aim to learn safe behaviors by intentionally guiding the demonstrator towards safety-critical states during offline demonstrations. Our key idea is to abstract the potential policy errors as an *adversarial disturbance* in the system that tries to push the agent towards safety-critical states over time. The corrective examples from these states allow the robot to learn how to safely recover when it deviates from the supervisor's distribution.

Specifically, during data collection, the demonstrator is guided towards critical states by the application of $\pi^G(x)$ as the input to the system instead of applying the demonstrator's action $\pi^*(x)$:

$$\pi^G(x) = \pi^*(x) + d(x), \quad (11)$$

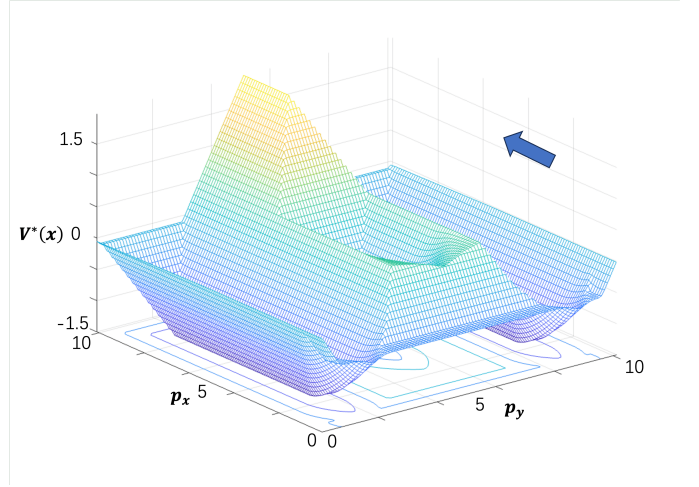


Fig. 1: The converged value function slice for 0° heading shown by the blue arrow, for the unicycle dynamics with $\bar{d} = 0.5$. The additive optimal disturbance on the control input $d^*(x)$ pushes the system towards $-\nabla V^*(x)$. Contours of the value function are plotted on p_x, p_y plane. The map of the environment can be seen in Fig. 3.

where $d(x)$ is the added disturbance. Intuitively, $d(x)$ steers the system closer to the BRT at each time step; correspondingly, expert will be taking actions to recover and avoid a potential collision, facilitating the learning of vital recovery maneuvers from these critical states.

Remark 1: It is important to note that the disturbance injected into the supervisor's policy simulates prediction errors occurring during testing, which is not necessarily adversarial. However, modeling it as an adversarial disturbance allows us to maintain system safety despite worst-case prediction errors that we might encounter during test time.

A key question that remains is how to compute $d(x)$? In this work, we use Hamilton-Jacobi reachability analysis to compute $d(x)$. Given the disturbance injection scheme in (11), the robot state evolution can approximately be described as $\dot{x} = f(x, u + d)$, where $d \in [-\bar{d}, \bar{d}]$. \bar{d} is a hyperparameter that can be used to control the amount of injected disturbance. We further discuss the impact of \bar{d} on the imitation performance in Sec. VI.

The expert controller could be used as the control policy $u(\cdot)$ for the reachability analysis to find the optimal disturbance policy $d(\cdot)$ specific to that expert. However, that would be impractical in an imitation learning setting as the HJ reachability computation would require querying the expert all around the state space. Instead, we compute the optimal disturbance, working against the optimal control policy that drives the system away from unsafe states. This results in a BRT that is a subset of all possible BRTs corresponding to different expert control policies. In order for any expert to fail it will first need to go into its own respective BRT then the BRT corresponding to the optimal control policy for safety. Hence, the computed disturbance is able to push all possible expert policies to safety critical states that are shared across all expert policies.

Given the disturbance-injected dynamics and the failure set

L , we compute the converged value function $V^*(x)$ in (8) by solving the HJI-VI in (4). $V^*(x)$ measures the closest a system can get to the failure set starting from the state x ; thus, it directly measures the safety criticality of the state x . Specifically, the smaller the $V^*(x)$, the more safety critical the state is. Given $V^*(x)$, we compute the corresponding optimal adversarial disturbance $d^*(x)$ in (10), which steers the system towards smallest $V^*(x)$, i.e., towards more safety-critical states. Finally, $d(x)$ is obtained by randomly scaling the magnitude of $d^*(x)$:

$$d(x) = d_{scale} \cdot d^*(x), \quad (12)$$

where $d_{scale} \sim U(0,1)$, which is a uniform distribution between $[0,1]$.

The scaling of the optimal adversarial disturbance helps in two ways: first, applying the optimal disturbance at each time step can steer the system too close to failure during the data collection procedure, which is not desirable for safety-critical systems. In contrast, randomizing the disturbance magnitude allows the demonstrator to complete its task successfully without causing the system to fail. Second, since we do not know the policy error encountered during testing beforehand, randomizing the disturbance magnitude results in more diverse demonstrations without being overly conservative.

Our overall data collection procedure is described in Algorithm 1. We then train a behavior cloning policy $\pi_\theta(x)$ on the collected data.

Algorithm 1: Safety Guided Data Collection

Input: Number of demonstrations K ; Trajectory length T

Output: Guided trajectory of states and corresponding expert actions $(x, \pi^*(x))$

for $i=1:K$ **do**

 Sample initial state x_1

for $j=1:T$ **do**

 Get optimal disturbance $d^*(x_i)$ using (10)

$d_{scale} \sim U(0,1)$

$d(x_i) \leftarrow d_{scale} * d^*(x_i)$

$\pi^G(x_i) \leftarrow \pi^*(x_i) + d(x_i)$,

 Store $(x_i, \pi^*(x_i))$ pair

 Apply $\pi^G(x_i)$ on the system to obtain the next state

x_{i+1}

end for

end for

return State and expert action pairs

VI. EXPERIMENTS

We demonstrate our method in two case studies: a ground robot navigating towards a goal position without colliding with obstacles and an autonomous aircraft taxiing task where an aircraft needs to taxi on a runway using RGB images from an onboard camera without steering off the runway.

To showcase that our method is agnostic to the demonstrator and imitator types, the imitation agent learns a state-based policy trained on a MPC-based expert controller for the ground navigation task, whereas the autonomous taxiing imitation agent learns a vision-based policy trained on a PID expert controller that has access to privileged state information during training (not available to the imitator).

We compare our methods against several offline and online imitation learning methods:

- **BC:** Behavior cloning with demonstrator rollout trajectories that are collected without any guidance, i.e., $d(x) = 0$.
- **Gaussian Noise BC:** Uncorrelated Gaussian noise injected into the demonstrator’s policy during data collection, i.e., $d(x) \sim N(0, \frac{\bar{d}^2}{4})$.
- **Uniform Noise BC:** I.i.d. uniform random noise injected into the demonstrator’s policy during data collection, i.e., $d(x) \sim U(-\bar{d}, \bar{d})$.
- **SAFE-GIL (ours):** Behavior cloning with safety-critical guidance during data collection.
- **Dagger- α :** Trajectories in the first α iterations are collected from the expert. Then the expert actions at the imitation policy rollout trajectories are aggregated iteratively.
- **Dagger SAFE-GIL(ours):** To show that our method is compatible with on policy imitation learning methods we implemented Dagger with guided trajectories. The guidance is applied both during the first α iterations guiding the expert and later guiding the imitation policy rollouts.

A. Safe Autonomous Navigation

We collect the expert demonstrations starting from the robot states with $p_x = 0$, $\theta = 0$ and p_y sampled uniformly in $[4.5, 5.5] m$. For the disturbance guidance as well as noise injection, we use $\bar{d} = 0.6 \bar{\omega}$, which corresponds to a maximum of up to 60% error in imitating the agent.

The imitation policy is modeled as an MLP that takes a transformed system state as input ($p_x, p_y, \sin(\theta)$ and $\cos(\theta)$) and outputs the angular velocity input to be applied on the robot. The MLP consists of 3 hidden layers with 128 neurons per layer and ReLU nonlinearity. The neural network (NN) weights were optimized using ADAM optimizer [19] for a total of 300 epochs with early stopping criteria on the validation loss with 50 epoch early stop patience.

We compare the success rates of the resulting imitation policies by rolling it out from 100 randomly sampled initial states between $p_y \in [4.8, 5.2] m$ with $p_x = 0$ and 0 heading. The success rate is defined as the percentage of initial states that reach the goal location without colliding with obstacles. Moreover, each imitator is trained on 10 different instance of data collection with different seeds to capture the performance variance of the method and the model training.

The mean success rates of different imitation policies as

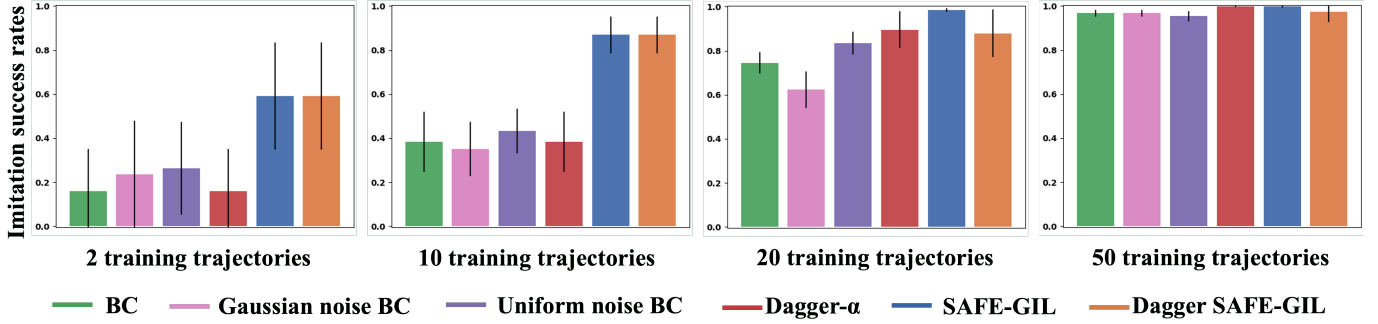


Fig. 2: Mean success rates and 95% CI of learned policy rollouts over 10 different instances of data collection and imitation learning as a function of the number of demonstration trajectories. Testing of the learned imitation policies is focused on the middle of the training initial condition region where it is critical to avoid the obstacle in the middle to reach the goal position. $\alpha = 5$ for both DAGger- α and DAGger SAFE-GIL. The proposed approach (SAFE-GIL) leads to a substantially higher success rate than other baselines with the same number of demonstrations.

a function of number of expert demonstrations are shown in Fig. 2. The imitation policy learned from safety-critical guidance data is able to achieve substantially higher success rate compared to other imitation policies, even with a small number of demonstrations (the success rate is $\sim 60\%$ with only 2 demonstrations and $\sim 87\%$ with 10 expert demonstrations). Achieving the same success rates requires more than 10 and 20 demonstrations with vanilla BC respectively, indicating a 2-5x improvement in data efficiency under the proposed approach. To understand the underlying reasons for this data efficiency, we illustrate the expert trajectories for vanilla BC and guided BC (top row), as well as the corresponding rollouts of the imitation policies (bottom row) in Fig. 3. Due to disturbance injection, the expert demonstrations

the proposed disturbance guidance some of these safety-critical states are never encountered by the expert, even as the number of collected expert trajectories increases. This can also be seen from the value distribution of states encountered by the expert under the proposed method and under vanilla BC. As shown in Fig. 4, the value distribution is shifted towards lower values, indicating a frequent visitation of safety-critical states during data collection. Finally, we note that the

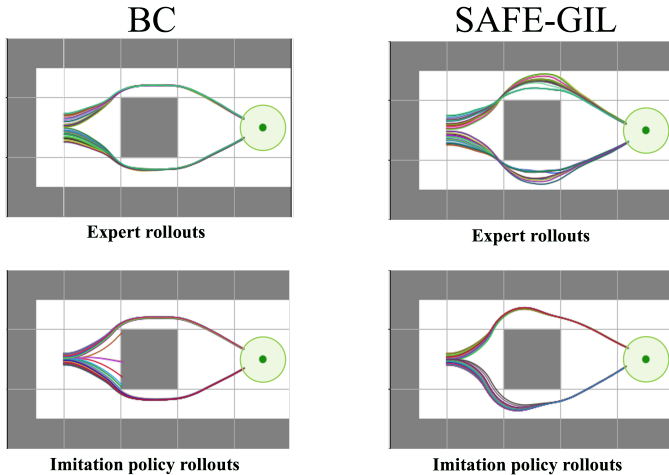


Fig. 3: Expert demonstrations (top row) and imitation policy rollouts (bottom row) corresponding to vanilla BC and the proposed method (SAFE-GIL). Collecting more expert trajectories without guidance generates more training data from similar states that have been previously observed. Intuitively, SAFE-GIL diversely guides the robot closer to the obstacles during training, allowing the imitator to recover from such states during the test time.

for the proposed method are guided closer to the obstacles; consequently, expert recovery maneuvers from these states are present in the demonstration data, allowing the learned imitation policy to better avoid the obstacles and the walls and achieving a higher success rate. On the other hand, without

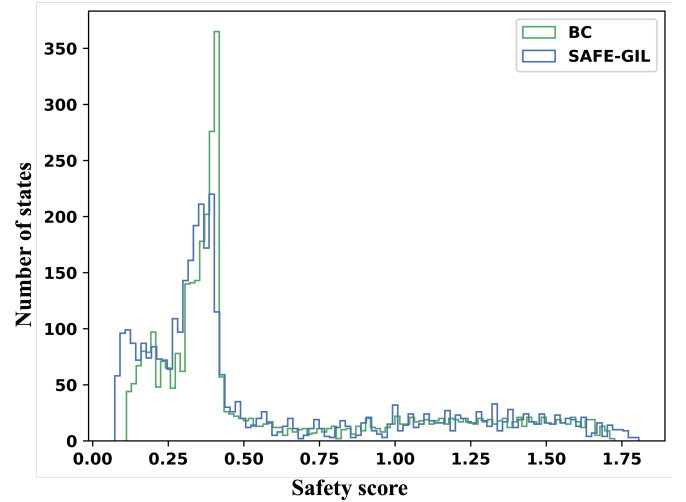


Fig. 4: Distribution of the safety scores ($V^*(x)$) of the states in the training set. A lower value means a more safety critical state. Guided data collection shifts the training distribution towards more safety critical states. Guided expert demonstrations visit safety critical states that have never been visited during expert demonstrations.

success rates of imitation policies corresponding to random noise injection during demonstration perform comparable to vanilla BC, highlighting the importance of adversarial nature of injected disturbance that guides the demonstrator to more safety-critical states.

Even though the proposed guidance mechanism is primarily intended for offline data collection, we also compare and combine our approach with online learning methods such as DAGger. Compared to DAGger, our guided methods show higher success rates for both case studies especially in the

low data regime. This is because in addition to simulating the imitation error our method actively guides the expert to more safety critical states. In contrast, DAgger addresses the compounding error problem but lacks the ability to guide to safety critical states.

Performance tradeoff. One of the inadvertent consequences of our approach is that the imitator learns from fewer samples from states maximizing the expert’s reward function as the training distribution shifts towards more safety critical states. This translates to worse learning in reward maximizing states and better learning in safety critical states. This can result in performance degradation compared to BC, especially when the actual imitation error in BC is not as high as the selected disturbance bound. This trade-off can be seen in Fig. 5. Here, we plot the average accumulated cost by the imitator

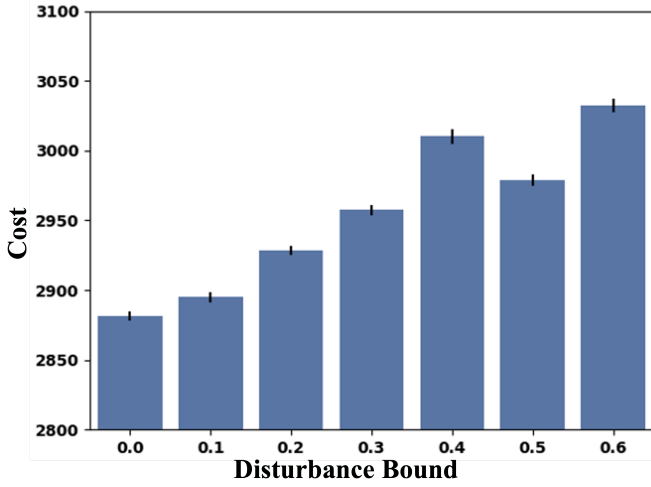


Fig. 5: The average and 95% CI of the cost (that the expert is optimizing for) of successful test trajectories of the imitation agents trained on data collected by SAFE-GIL for different disturbance bounds (trained on 50 demonstrations). SAFE-GIL with $\bar{d} = 0$ reduces to BC. The results are averaged over 10 seeds. The proposed approach leads to a slight performance degradation in exchange of safety enhancement.

policy along the successful trajectories. The accumulated cost increases for the proposed method as the disturbance bound increases. Specifically, for a disturbance bound of 0.6, there is a $\sim 5\%$ degradation in the performance compared to vanilla BC method.

Effect of disturbance bound. The guidance of the demonstrator, and therefore, the learning of the safety-critical behavior, is highly dependent on the choice of the disturbance bound. Thus, we perform an ablation study to understand the effect of the disturbance bound on the success rate of SAFE-GIL. The corresponding results are shown in Fig. 6. As the disturbance bound increases, the proposed method is able to expose the demonstrator to potential higher learning errors (modeled as disturbance) and guide it towards more unsafe states. This results in the extraction of the expert’s actions in those states and, therefore, the learning of the recovery behavior by the imitation agent. Thus, a higher disturbance

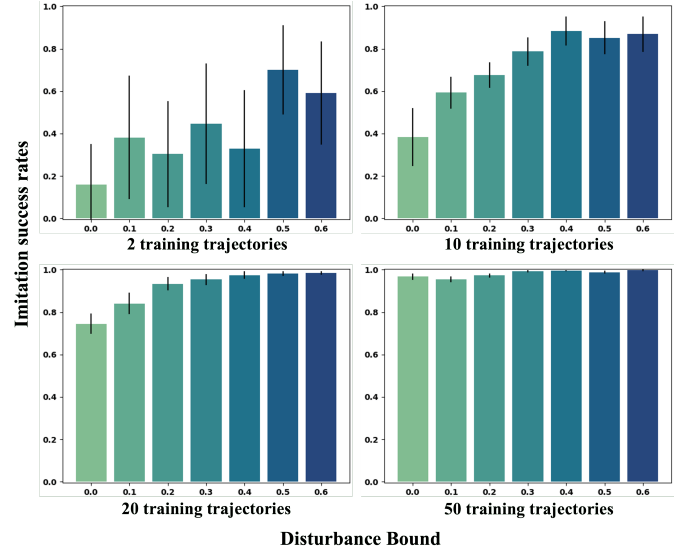


Fig. 6: Mean success rates over 10 imitation policies with different seeds as a function of the number of demonstration trajectories, plotted for SAFE-GIL with decreasing \bar{d} values. SAFE-GIL with $\bar{d} = 0$ reduces to BC. The success rates are increasing with increasing \bar{d} values.

bound results in a better and safer imitation policy, especially when the number of demonstrations is very small (and hence the imitation error will likely be higher). However, increasing the disturbance bound beyond a particular point leads the system to states that are too risky, which the expert might fail to recover from, causing the system to fail. The choice of disturbance bound is thus a critical hyperparameter for the proposed method, which we discuss further in Sec. VII.

B. Autonomous Taxiing Example

The second case study is an aircraft taxiing problem, used as a benchmark for robust perception and verification in [18, 17, 10]. The agent is a Cessna 208B Grand Caravan utility aircraft simulated in an X-Plane flight simulator on runway 04 of Grant County International Airport. The system dynamics are modeled as:

$$\dot{p}_x = v \sin(\theta), \quad (13)$$

$$\dot{p}_y = v \cos(\theta), \quad (14)$$

$$\dot{\theta} = (v/h) \tan(\omega) \quad (15)$$

The robot state is given by $x := (p_x, p_y, \theta)$, where (p_x, p_y, θ) denote the crosstrack error (CTE), the downtrack position (DTP), and the heading error (HE) with respect to the runway centerline, respectively. v is the constant 5 m/s velocity of the aircraft. The length of the aircraft, h is 5 m . The robot control input is given by its steering angle $u := \omega$, which is bounded by $\omega \in [-\bar{\omega}, \bar{\omega}]$. In our example, we use $\bar{\omega} = 1 \text{ rad/s}$. The task is to reach the end of the runway $p_y = 200$ without going out of the runway. The task needs to be performed autonomously using the RGB images captured through a camera mounted on the plane’s right wing (example image in Fig. 8).

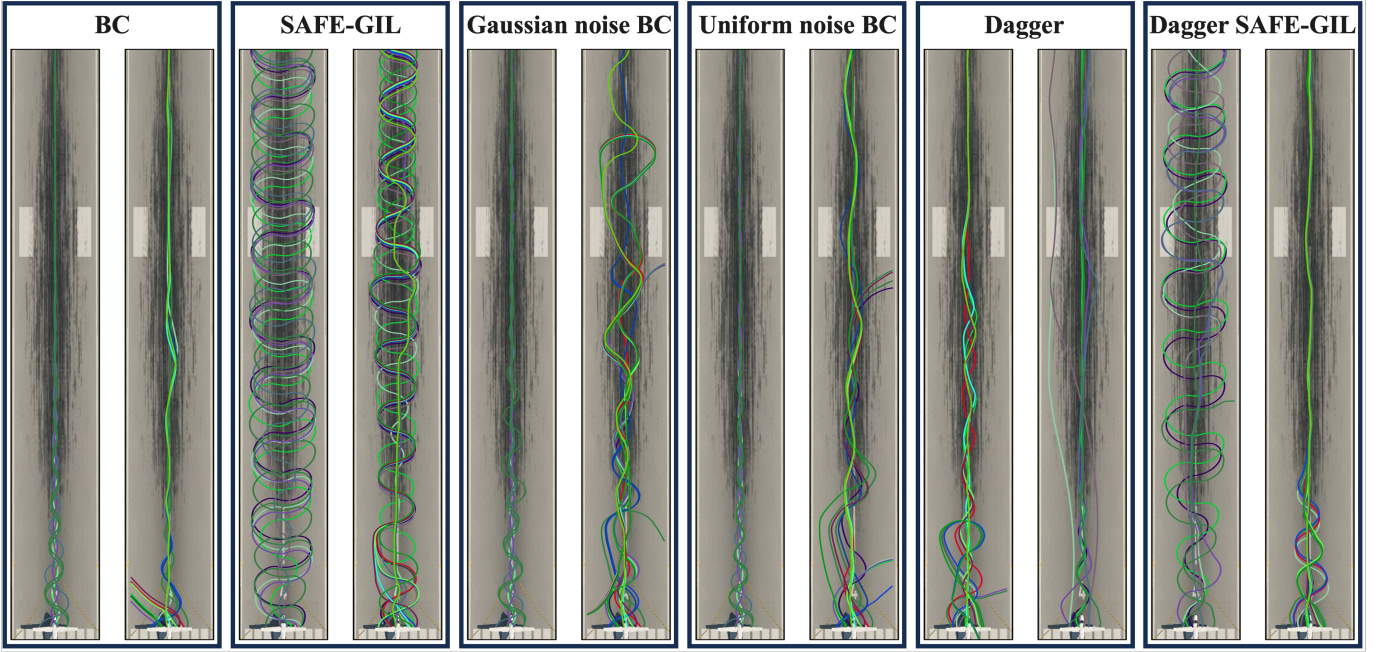


Fig. 7: Expert demonstrations (left) and imitation policy rollouts (right) corresponding to BC, SAFE-GIL, Gaussian noise BC, Uniform noise BC, Dagger, and Dagger SAFE-GIL. Unguided expert rollouts visit the same optimal states. Guided expert rollouts visit a wide range of states of different safety criticality. This results in learned policy rollouts that take longer to finish the task but are safer. Injecting random noise during expert demonstrations doesn't change the distribution of the collected states substantially. Dagger is able to recover from the learning errors in the learned policy when deployed from the same conditions as the training, however it doesn't learn the expert policy in safety critical states. Dagger SAFE-GIL collects data from on policy learning errors and with further guidance towards more safety critical states. This results in a high performance policy and learning of the expert behavior in safety critical conditions at the same time.

Expert is a proportional controller $u = \tan(-0.74p_x - 0.44\theta)$ designed to keep the aircraft inside the runway and steer towards the centerline. The expert has privileged access to the crosstrack error and heading error during the data collection procedure, which is not available to the imitator. Instead, it needs to imitate the expert based on onboard RGB images. The unsafe states for the aircraft are defined as $L = \{x : |p_x| \geq 10\}$, corresponding to the plane leaving the runway.

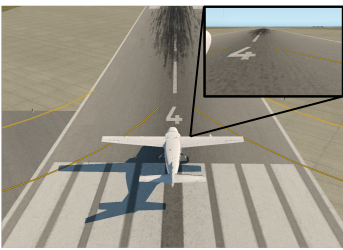


Fig. 8: An example RGB image from the right wing of the aircraft captured from X-Plane flight simulator.

The imitation policy is modeled as an MLP, which consists of 4 hidden layers with 128 neurons per layer and ReLU nonlinearity, that takes a preprocessed RGB image as input and outputs the steering angle to be applied on the aircraft. The neural network (NN) weights were optimized using ADAM optimizer [19]

for a total of 500 epochs with early stopping criteria on the validation loss with 50 epoch early stop patience.

The demonstration initial conditions are sampled uniformly between $p_x \in [-5, 5]m$, $\theta \in [-30^\circ, 30^\circ]$ with $p_y = 0$. For the disturbance guidance and noise injection, we use $\bar{d} = 0.5 \bar{\omega}$, which corresponds to a maximum of up to 50% error in imitating the agent.

We test the imitation policies by rolling them out from

16 randomly sampled initial states between $p_x \in [-7, -5]$, $\theta \in [-60^\circ, -30^\circ]$ and $p_x \in [5, 7]$, $\theta \in [30^\circ, 60^\circ]$, with $p_y \in [80, 150]$ which corresponds to the aircraft being close to the runway boundary and heading towards it. Moreover, starting from $p_y = 100$, the centerline starts disappearing due to the skidmarks on the runway which makes the task of vision-based navigation even harder. Testing the imitation policies starting from challenging conditions allows us to compare the safety capability and robustness of each method. The success rate is defined as the percentage of initial states that reach the end of the runway without going out of the boundaries. Moreover, each imitator is trained for 5 different seeds to capture the performance variance.

The mean success rates of different imitation policies as a function of the number of expert demonstrations are shown in Fig. 9. The imitation policy learned from safety-critical guidance data achieves substantially higher success rate compared to other methods including on policy DAGger with as low as 2 demonstration trajectories. This highlights the effectiveness of the safety guidance for learning safe and robust imitation policies. We believe the substantial difference between our method and the rest comes from the exploration of safety critical states in the visual manifold. Although the safety guidance is in regard to the constraints in the state space and the modeled dynamics of the agent, it also allows for the observation of unsafe states in the visual manifold. In this case, as seen in Fig. 7, the disturbance guides the expert towards the runway side markings seen in Fig. 8, hence even with 2 expert trajectories, the agent is able to learn to correct its heading when it observes the runway side markings. Therefore,

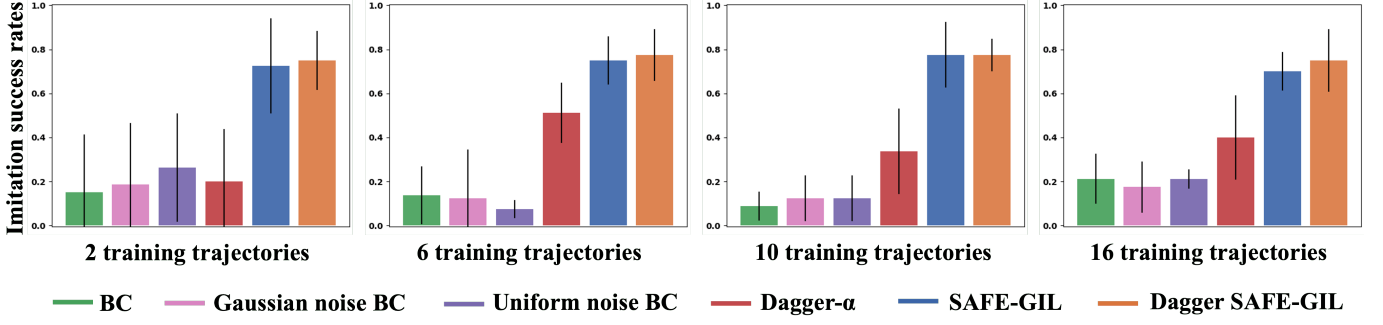


Fig. 9: Mean success rates and 95% CI over 5 imitation policies with different seeds as a function of the number of demonstration trajectories. The test initial conditions are sampled from positions close to the runway boundary and the aircraft heading towards it, to test the learned policies performance under safety critical conditions. $\alpha = 1$ for both DAGger- α and DAGger SAFE-GIL. The proposed approach (SAFE-GIL) leads to a substantially higher success rate than other baselines with as low as 2 demonstrations.

the imitator learns a safe policy in the visual manifold of the training set.

Shift in training data distribution. We plot the value distribution of the states encountered by the guided and unguided expert in Fig. 10. We observe that the distribution is very different between the guided and the vanilla expert. The vanilla expert’s distribution is concentrated on a small region of safety criticality level, whereas the guided expert covers a much more diverse and safety critical state distribution. Even as the number of trajectories increases, the expert visits the same states, which maximize its performance, as seen in Fig. 7.

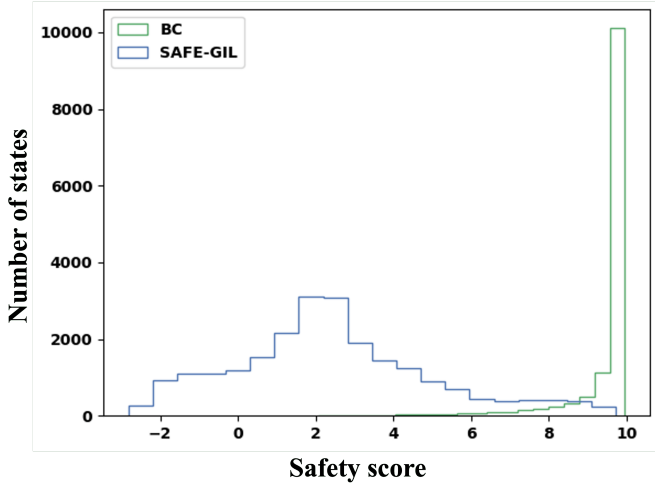


Fig. 10: Distribution of the safety scores ($V^*(x)$) of the states in the training set. A lower value means a more safety critical state. Guided data collection shifts the training distribution towards more safety critical states. Guided expert demonstrations accumulate training data concentrated into a small region of safety level. Since the expert prefers the trajectories maximizing its reward, it visits similar states maximizing it, for all demonstrations. Therefore, collecting more data does not result in more diverse demonstrations. SAFE-GIL collects expert actions from a wider range of safety criticality level, as it visits safety critical states that have never been seen during unguided expert demonstrations.

Performance tradeoff. In Fig. 11, we plot the time it takes for the imitation agents to successfully arrive at the end of the runway. The adversarial disturbance pushes the expert to the sides of the runway and to higher HE during data collection, as seen in Fig. 7 therefore, our method is not able to collect

data on observations with small HE along the centerline and the corresponding expert action of steering in alignment with the centerline. This results in the imitation policy not being able to correct its heading when it sees the centerline and swirl from side to side on the runway taking longer to cross it. The time it takes to complete the task increases with the magnitude of the disturbance bound up to $\sim 10\%$ compared to the vanilla BC.

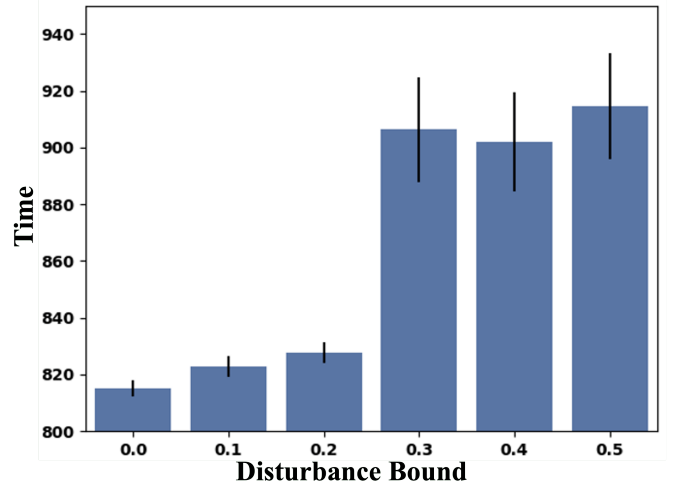


Fig. 11: The average and 95% CI of the time of task completion of successful test trajectories of the imitation agents trained on data collected by SAFE-GIL for different disturbance bounds (trained on 16 demonstrations). SAFE-GIL with $\bar{d} = 0$ reduces to BC. The results are averaged over 5 seeds. The proposed approach leads to a slight performance degradation in exchange of safety enhancement.

Effect of disturbance bound. In Fig. 12 we plot the percentage of successful imitation rollouts from test initial states as a function of number of training trajectories for different disturbance bounds on the guidance. The increase of disturbance bound allows the expert to be guided to more diverse demonstrations and also towards more unsafe states. The resulting training data for imitation has more number of states critical for safety and less number of states critical for performance. This results in lower task failure rate as seen in Fig. 12 at the expense of performance as seen on Fig. 11.

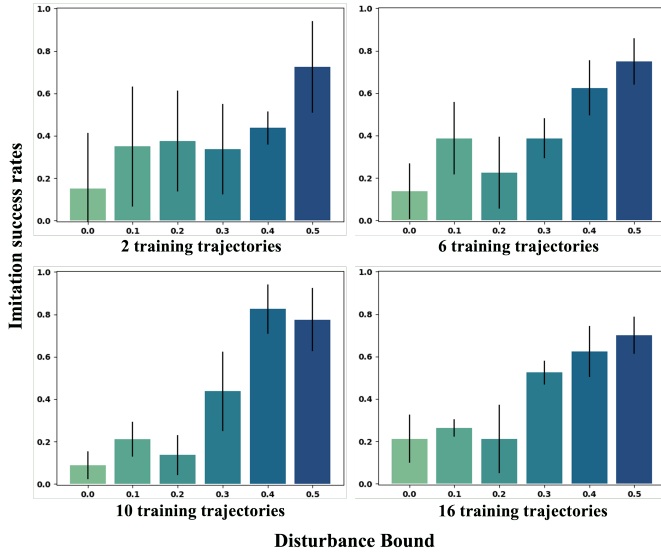


Fig. 12: Mean success rates over 5 imitation policies with different seeds as a function of the number of demonstration trajectories, plotted for SAFE-GIL with decreasing \bar{d} values. SAFE-GIL with $\bar{d} = 0$ reduces to BC. The success rates are increasing with increasing \bar{d} values.

VII. DISCUSSION AND FUTURE WORK

We propose a HJ reachability-based framework to guide the demonstrator trajectories towards more safety critical states and teach the imitation policy how to recover from the states that are risky. We demonstrate that the proposed guided data collection scheme results in significantly higher success rates, especially in low data regimes where the prediction error in the imitation policy might be high. This comes with a tradeoff on performance since our method biases training to more closely replicate expert behavior in safety critical states and allows more variance in less critical states.

A limitation of the proposed method is that it requires an informed selection of disturbance bound, which either requires prior familiarity with the expert agent or tuning by the designer during expert demonstrations. In the future, we will use a combination of off-policy and on-policy methods to estimate the disturbance bound in an informed manner. Our method also relies on HJ reachability and a dynamics model of the robot to compute the injected disturbance. We hypothesize that an approximate dynamics model should be sufficient for the disturbance calculation, which we will explore further in the future. Finally, we are excited to apply our framework to a broader range of robotics applications and systems, including real robotic testbeds.

ACKNOWLEDGMENTS

This work is supported in part by the NSF CAREER Program under award 2240163 and the DARPA ANSR program.

REFERENCES

[1] A. D. Ames, X. Xu, J. W. Grizzle, and P. Tabuada. Control barrier function based quadratic programs for

safety critical systems. *IEEE Transactions on Automatic Control*, 62(8):3861–3876, 2017.

[2] Andrea Bajcsy, Somil Bansal, Eli Bronstein, Varun Tolani, and Claire J Tomlin. An efficient reachability-based framework for provably safe autonomous navigation in unknown environments. In *IEEE Conference on Decision and Control (CDC)*, 2019.

[3] Mayank Bansal, Alex Krizhevsky, and Abhijit S. Ogale. Chauffeurnet: Learning to drive by imitating the best and synthesizing the worst. *ArXiv*, abs/1812.03079, 2018.

[4] Somil Bansal and Claire J. Tomlin. Deepreach: A deep learning approach to high-dimensional reachability. In *2021 IEEE International Conference on Robotics and Automation (ICRA)*, pages 1817–1824, 2021. doi: 10.1109/ICRA48506.2021.9561949.

[5] Somil Bansal, Mo Chen, Sylvia Herbert, and Claire J Tomlin. Hamilton-Jacobi Reachability: A brief overview and recent advances. In *IEEE Conference on Decision and Control (CDC)*, 2017.

[6] Somil Bansal, Mo Chen, Sylvia Herbert, and Claire J Tomlin. Hamilton-jacobi reachability: A brief overview and recent advances. In *2017 IEEE 56th Annual Conference on Decision and Control (CDC)*, pages 2242–2253. IEEE, 2017.

[7] Somil Bansal, Varun Tolani, Saurabh Gupta, Jitendra Malik, and Claire Tomlin. Combining optimal control and learning for visual navigation in novel environments. In *Conference on Robot Learning (CoRL)*, 2019.

[8] Somil Bansal, Mo Chen, Ken Tanabe, and Claire J Tomlin. Provably safe and scalable multivehicle trajectory planning. *IEEE Transactions on Control Systems Technology (TCST)*, 29(6):2473–2489, 2020.

[9] Javier Borquez, Kaustav Chakraborty, Hao Wang, and Somil Bansal. On safety and liveness filtering using hamilton-jacobi reachability analysis. *arXiv preprint arXiv:2312.15347*, 2023.

[10] Taejoon Byun and Sanjai Rayadurgam. Manifold for machine learning assurance. *2020 IEEE/ACM 42nd International Conference on Software Engineering: New Ideas and Emerging Results (ICSE-NIER)*, pages 97–100, 2020.

[11] Felipe Codevilla, Matthias Müller, Alexey Dosovitskiy, Antonio M. López, and Vladlen Koltun. End-to-end driving via conditional imitation learning. *2018 IEEE International Conference on Robotics and Automation (ICRA)*, pages 1–9, 2017.

[12] Chelsea Finn, Tianhe Yu, Tianhao Zhang, P. Abbeel, and Sergey Levine. One-shot visual imitation learning via meta-learning. *ArXiv*, abs/1709.04905, 2017.

[13] Ryan Hoque, Ashwin Balakrishna, Ellen R. Novoseller, Albert Wilcox, Daniel S. Brown, and Ken Goldberg. Thriftydagger: Budget-aware novelty and risk gating for interactive imitation learning. In *Conference on Robot Learning*, 2021.

[14] Ryan Hoque, Ashwin Balakrishna, Carl Putterman, Michael Luo, Daniel S. Brown, Daniel Seita, Brijen

- Thananjeyan, Ellen R. Novoseller, and Ken Goldberg. Lazydagger: Reducing context switching in interactive imitation learning. *2021 IEEE 17th International Conference on Automation Science and Engineering (CASE)*, pages 502–509, 2021.
- [15] Kai-Chieh Hsu, Haimin Hu, and Jaime Fernández Fisac. The safety filter: A unified view of safety-critical control in autonomous systems. *arXiv preprint arXiv:2309.05837*, 2023.
- [16] Sandy H Huang, Kush Bhatia, Pieter Abbeel, and Anca D Dragan. Establishing appropriate trust via critical states. In *2018 IEEE/RSJ International Conference on Intelligent Robots and Systems (IROS)*, pages 3929–3936. IEEE, 2018.
- [17] Kyle D. Julian, Ritchie Lee, and Mykel J. Kochenderfer. Validation of image-based neural network controllers through adaptive stress testing. *2020 IEEE 23rd International Conference on Intelligent Transportation Systems (ITSC)*, pages 1–7, 2020.
- [18] Sydney M. Katz, Anthony Corso, Christopher A. Strong, and Mykel J. Kochenderfer. Verification of image-based neural network controllers using generative models. *2021 IEEE/AIAA 40th Digital Avionics Systems Conference (DASC)*, pages 1–10, 2021.
- [19] Diederik P. Kingma and Jimmy Ba. Adam: A method for stochastic optimization. *CoRR*, abs/1412.6980, 2014.
- [20] Oliver Kroemer, Scott Niekum, and George Dimitri Konidaris. A review of robot learning for manipulation: Challenges, representations, and algorithms. *J. Mach. Learn. Res.*, 22:30:1–30:82, 2019.
- [21] Aviral Kumar, Joey Hong, Anikait Singh, and Sergey Levine. Should i run offline reinforcement learning or behavioral cloning? In *International Conference on Learning Representations*, 2022. URL <https://openreview.net/forum?id=AP1MKT37rJ>.
- [22] Michael Laskey, Jonathan Lee, Roy Fox, Anca D. Dragan, and Ken Goldberg. Dart: Noise injection for robust imitation learning. In *Conference on Robot Learning*, 2017.
- [23] Kunal Menda, K. Driggs-Campbell, and Mykel J. Kochenderfer. Ensembledagger: A bayesian approach to safe imitation learning. *2019 IEEE/RSJ International Conference on Intelligent Robots and Systems (IROS)*, pages 5041–5048, 2018.
- [24] I. Mitchell. A toolbox of level set methods. <http://www.cs.ubc.ca/mitchell/ToolboxLS/toolboxLS.pdf>, Tech. Rep. TR-2004-09, 2004.
- [25] Ian Mitchell, Alex Bayen, and Claire J. Tomlin. A time-dependent Hamilton-Jacobi formulation of reachable sets for continuous dynamic games. *IEEE Transactions on Automatic Control (TAC)*, 50(7):947–957, 2005.
- [26] Ian M. Mitchell. A toolbox of level set methods. 2005.
- [27] Ian M. Mitchell and Claire J. Tomlin. Level set methods for computation in hybrid systems. In *International Conference on Hybrid Systems: Computation and Control*, 2000.
- [28] Yunpeng Pan, Ching-An Cheng, Kamil Saigol, Keuntaek Lee, Xinyan Yan, Evangelos A. Theodorou, and Byron Boots. Agile autonomous driving using end-to-end deep imitation learning. *Robotics: Science and Systems XIV*, 2017.
- [29] Dean A. Pomerleau. Alvin, an autonomous land vehicle in a neural network. 2015.
- [30] Stephane Ross and Drew Bagnell. Efficient reductions for imitation learning. In Yee Whye Teh and Mike Titterton, editors, *Proceedings of the Thirteenth International Conference on Artificial Intelligence and Statistics*, volume 9 of *Proceedings of Machine Learning Research*, pages 661–668, Chia Laguna Resort, Sardinia, Italy, 13–15 May 2010. PMLR. URL <https://proceedings.mlr.press/v9/ross10a.html>.
- [31] Stephane Ross, Geoffrey Gordon, and Drew Bagnell. A reduction of imitation learning and structured prediction to no-regret online learning. In Geoffrey Gordon, David Dunson, and Miroslav Dudík, editors, *Proceedings of the Fourteenth International Conference on Artificial Intelligence and Statistics*, volume 15 of *Proceedings of Machine Learning Research*, pages 627–635, Fort Lauderdale, FL, USA, 11–13 Apr 2011. PMLR. URL <https://proceedings.mlr.press/v15/ross11a.html>.
- [32] Ameesh Shah, Jonathan DeCastro, John Gideon, Beyazit Yalcinkaya, Guy Rosman, and Sanjit A. Seshia. Specification-guided data aggregation for semantically aware imitation learning, 2023.
- [33] Kim P. Wabersich, Andrew J. Taylor, Jason J. Choi, Koushil Sreenath, Claire J. Tomlin, Aaron D. Ames, and Melanie N. Zeilinger. Data-driven safety filters: Hamilton-Jacobi reachability, control barrier functions, and predictive methods for uncertain systems. *Preprint*, 2023.
- [34] Maryam Zare, Parham Mohsenzadeh Kebria, Abbas Khosravi, and Saeid Nahavandi. A survey of imitation learning: Algorithms, recent developments, and challenges. *ArXiv*, abs/2309.02473, 2023.
- [35] Jiakai Zhang and Kyunghyun Cho. Query-efficient imitation learning for end-to-end simulated driving. In *AAAI Conference on Artificial Intelligence*, 2017.